Lifetime measurements of states in ^{15}O

N. Galinski,[1,2,*] S. K. L. Sjue,[1] G. C. Ball,[1] D. S. Cross,[1] B. Davids,[1] H. Al Falou,[3] A. B. Garnsworthy,[1] G. Hackman,[1] U. Hager,[1] D. A. Howell,[1,2] M. Jones,[4] R. Kanungo,[3] R. Kshetri,[1] K. G. Leach,[5] J. R. Leslie,[6] M. Moukaddam,[1] J. N. Orce,[1,7] E. T. Rand,[5] C. Ruiz,[1] G. Ruprecht,[1] M. A. Schumaker,[5] C. E. Svensson,[5] S. Triambak,[1,7,8] and C. D. Unsworth[1]

[1]*TRIUMF, Vancouver, British Columbia, Canada*
[2]*Department of Physics, Simon Fraser University, Burnaby, British Columbia, Canada*
[3]*Department of Astronomy and Physics, Saint Mary's University, Halifax, Nova Scotia, Canada*
[4]*Department of Physics, University of Liverpool, Liverpool, United Kingdom*
[5]*Department of Physics, University of Guelph, Guelph, Ontario, Canada*
[6]*Department of Physics, Queens University, Kingston, Ontario, Canada*
[7]*Department of Physics, University of the Western Cape, South Africa*
[8]*iThemba Laboratory for Accelerator Based Sciences, Somerset West 7129, South Africa*

(Received 25 April 2014; revised manuscript received 2 July 2014; published 5 September 2014)

At low stellar temperatures the energy release due to the CN cycle is regulated by its slowest reaction ^{14}N$(p,\gamma)^{15}$O, the rate of which strongly depends on the subthreshold resonance at $E_{\text{c.m.}} = -504$ keV, which corresponds to the 6.79 MeV state in ^{15}O. By using the Doppler-shift attenuation method and the ^{3}He$(^{16}$O$,\alpha)^{15}$O reaction to populate the state, we obtained an upper limit on the lifetime of this state of $\tau < 1.8$ fs [68.3% confidence level (C.L.)]. In addition we measured the lifetimes of the 6.18 and 6.86 MeV states to be $\tau < 2.5$ and $\tau = 13.3^{+0.9}_{-1.2}$ fs, respectively (68.3% C.L.), in good agreement with the literature.

DOI: 10.1103/PhysRevC.90.035803 PACS number(s): 21.10.Tg, 26.20.−f

I. INTRODUCTION

Hydrogen burning in stars proceeds via the *pp* chain and the CNO cycle. If the catalysts C or N are present, the CNO cycle dominates for temperatures $T > 0.02$ GK, which correspond to Gamow peak center-of-mass (c.m.) energies $E_{\text{c.m.}} > 30$ keV. Hence the CNO cycle dominates energy production for main sequence (MS) stars a bit more massive than the sun, all stars at the end of their MS lifetimes, and stars on the red-giant branch. The slowest process in the cycle ^{14}N$(p,\gamma)^{15}$O affects the amount of He ash produced and regulates the energy generation [1], which affects the time scale of the MS evolution. This has several astrophysical implications. The age of a globular cluster can be determined via the luminosity of its stars at the MS turnoff [2,3], which depends on the ^{14}N$(p,\gamma)^{15}$O reaction rate. This reaction also determines the rate at which He is produced in the H-burning shell of red-giant stars, which affects further nucleosynthesis of heavier elements. The neutrino fluxes of CN cycle nuclei provide information on the interior structure of the sun and are measurable with SNO+ [4]. A precise determination of the ^{14}N$(p,\gamma)^{15}$O reaction rate would reduce this nuclear input uncertainty of the CNO neutrino fluxes, currently estimated to be ±7.2% [5].

The first study of this reaction over a wide range of energies $E_{\text{c.m.}} = 170$–3360 keV was reported in Ref. [6]. Figure 1 shows the level structure of ^{15}O around the ^{14}N + p threshold [7]. Extrapolations of the S factor down to zero energy found the capture into the ground state (g.s.) with $S_{\text{g.s.}}(0) = 1.55 \pm 0.34$ keV b to be comparable to the capture into the $E_{\text{c.m.}} = -504$ keV subthreshold resonance that corresponds to the 6.79 MeV state in ^{15}O with $S_{6.79}(0) = 1.41 \pm 0.02$ keV b. However, reanalysis of these data with R-matrix fits by the authors of Ref. [8] led to a dramatically different extrapolation with $S_{\text{g.s.}}(0) = 0.08^{+0.13}_{-0.06}$ and $S_{6.79}(0) = 1.63 \pm 0.17$ keV b, which resulted in a negligible ground-state contribution. This essentially halves the reaction rate, which is proportional to the total S factor. Recent experiments at $E_{\text{c.m.}} = 65$–445 keV [9–12] have also found a small ground-state contribution that ranges from $S_{\text{g.s.}}(0) = 0.15$–$0.49$ keV b with most of the difference due to differing treatments of high-lying unmeasured resonances. Reference [5] estimates the uncertainties in $S_{\text{g.s.}}(0)$ and $S_{\text{total}}(0)$ to be 19% and 7%, respectively.

In order to better constrain R-matrix fits new measurements of the radiative width Γ_γ of the subthreshold 6.79 MeV state in ^{15}O are desirable. In this case the total width is $\Gamma = \Gamma_\gamma$ since this state decays 100% of the time to the ground state by γ-ray emission. Reference [6] used $\Gamma_\gamma = 6.3$ eV, whereas the fitted radiative width reported in Ref. [8] was $\Gamma_\gamma = 1.75 \pm 0.60$ eV. This has prompted direct Γ_γ measurements, one of which [13] points to an even smaller radiative width. This width can be measured via Coulomb excitation or obtained from the lifetime τ since they are related via the equation $\Gamma = \hbar/\tau$. The first of these measurements, Ref. [13], was a lifetime measurement that used the Doppler-shift attenuation method (DSAM), which reported a value of $\Gamma_\gamma = 0.41^{+0.34}_{-0.13}$ eV. However, by using the same method $\Gamma_\gamma > 0.85$ eV was reported in Ref. [14] in slight disagreement. The authors of Ref. [14] have reduced the statistical and systematic uncertainties in comparison with Ref. [13] with higher statistics and γ-ray measurements at more angles. There was an attempt to obtain Γ_γ via the Coulomb excitation method [15], but no distinct γ rays from the 6.79 MeV state were observed. The result was an upper limit of $\Gamma_\gamma = 0.95^{+0.06}_{-0.95}$ eV. The current experimental situation is unsatisfactory, which motivates additional measurements.

*naomi.galinski@gmail.com

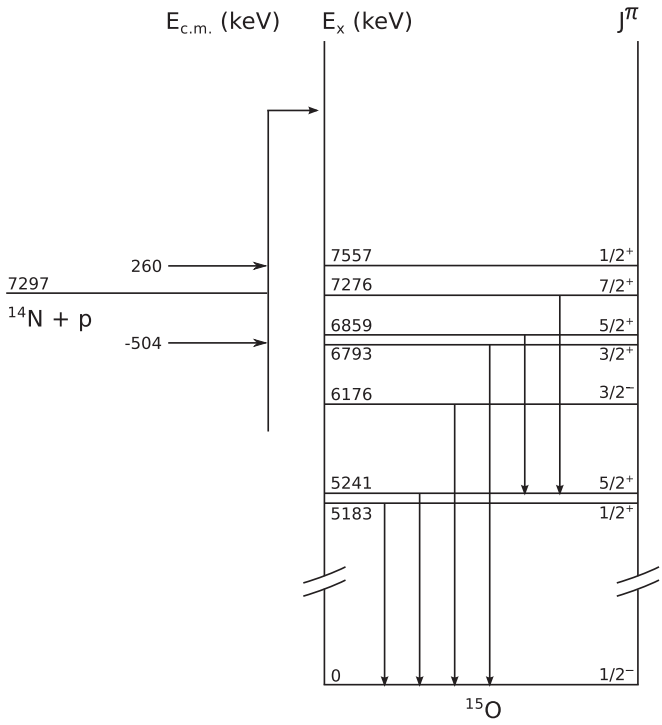

FIG. 1. Level structure of ^{15}O [7]. Transitions observed in this measurement are indicated.

Here we report a lifetime measurement which used the DSAM [16]. Such measurements can be performed if the slowing down time of the recoiling nucleus in a stopper is comparable to the lifetime of the excited state. The recoil speed changes as it slows down in a stopping medium, and therefore the Doppler shift of the γ ray depends on the time of decay. The time-dependent Doppler-shifted energy of the emitted γ ray is

$$E_\gamma = E_\gamma^0 \frac{\sqrt{1-\beta(t)^2}}{1-\beta(t)\cos\theta}, \quad (1)$$

where E_γ^0 is the emitted γ-ray energy in the recoil rest frame, $\beta(t)$ is the time-dependent speed in units of the speed of light, and θ is the laboratory angle between the emitted γ ray and the recoil. In this way the Doppler shift is related to the lifetime of the recoil. To achieve an accurate lifetime one has to know the stopping power of the recoiling ion in the stopping medium since this will determine $\beta(t)$.

A centroid shift analysis extracts a lifetime from measured Doppler-shifted γ-ray centroids at different angles. Another way to extract the lifetime is by performing a line-shape analysis, which we have adopted. In addition to a centroid shift there is a unique γ-ray line shape associated with each lifetime. If the recoil speed is large enough and the Doppler spread is greater than the intrinsic detector resolution, then a line-shape analysis is possible. In this experiment the ^{3}He(^{16}O,α)^{15}O reaction was used to populate the 6.79 MeV and other states in ^{15}O.

Both Refs. [13,14] used centroid shift analyses, which yielded lifetimes of $\tau = 1.60^{+0.75}_{-0.72}$ fs [90% confidence level (C.L.)] and an upper limit of $\tau < 0.77$ fs, respectively. Only statistical uncertainties are reported in these final results. They used the same reaction to populate the 6.79 MeV state in ^{15}O, and their ^{15}O recoil speeds were $\beta < 0.002$. At these speeds, nuclear stopping powers, which are difficult to measure and calculate theoretically, dominate over electronic stopping powers. The total uncertainty in the inferred lifetime due to the stopping power uncertainty is not mentioned in Ref. [13], but a 100% increase in the lifetime up to 3.2 ± 1.5 fs is mentioned if the density of the target was that of TaN with N occupying substitutional lattice sites instead of that of pure Ta, which they used in their analysis. In Ref. [14] the same uncertainty in stopping powers due to the target density was reported to result in only a 2% increase in the upper limit on the lifetime. Due to inverse kinematics we had a higher initial recoil speed $\beta = 0.05$, so the recoil is slowing down in the electronic stopping region when the γ ray is emitted; electronic stopping powers can be calculated and measured reliably.

II. EXPERIMENTAL PROCEDURE

The DSAM experiment was performed by using the Doppler-Shift Lifetimes (DSL) chamber in the ISAC-II facility at TRIUMF. A stable ^{16}O beam was accelerated to 50 MeV

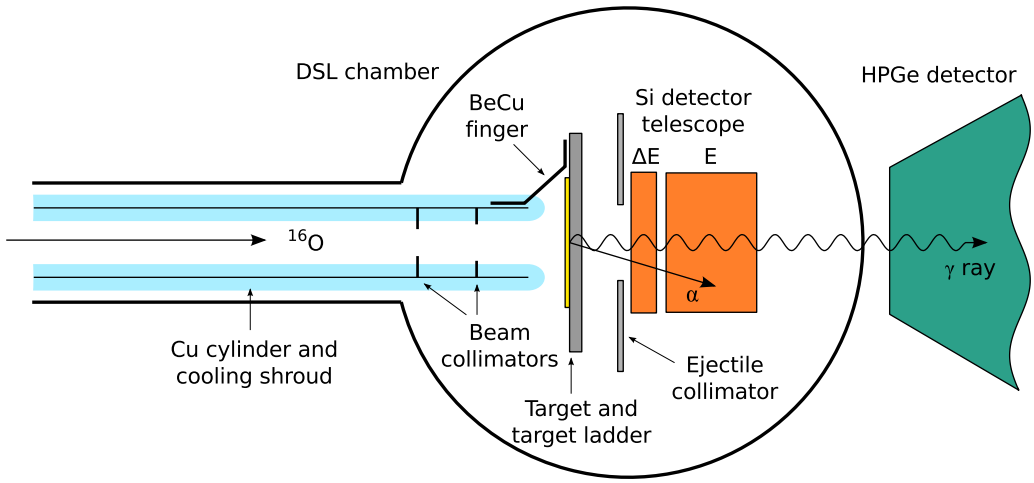

FIG. 2. (Color online) Schematic of the experimental setup.

and bombarded a ^{3}He-implanted Au-foil target to populate the level of interest in ^{15}O via the ^{3}He(^{16}O,α)^{15}O reaction. Figure 2 shows a schematic of the experiment. The beam had an average current of 40 nA with a charge state of 5^+ (equivalent to 5×10^{10} ion s^{-1}), a 1σ energy spread of $\pm 0.1\%$, and a beam spot diameter of 3.0 mm that contains 90% of the beam. The beam passed through two collimators with diameters of 2.5 and 3.0 mm at distances of 73 and 49 mm, respectively, upstream from the target. The maximum recoil speed was approximately $0.055c$, which varied slightly depending on the Q values of the individual resonances.

Deexcitation γ rays were detected in coincidence with α-particle ejectiles by using a TIGRESS detector centered at 0° with respect to the beam axis. A TIGRESS γ-ray detector is a clover detector with four high-purity germanium (HPGe) crystals [17]. Its front surface was located 14.88 cm from the target, and it subtended a maximum angle of 21.6° from the beam axis. The absolute photopeak efficiency in the add-back mode for 7.2 MeV γ rays at 14.88 cm is 0.092% as calculated by a GEANT4 simulation [18,19]. The add-back mode used to read out the data creates an event-by-event summed spectrum of the energy deposited in all four Ge crystals and enhances the full energy peak detection efficiency compared to single-crystal hits [20]. Lifetimes were inferred from a line-shape analysis of this add-back spectrum. The gain stability of the detector and electronics was checked by using transitions in ^{197}Au and ^{15}O, which were not Doppler shifted. No gain shift was observed in the 279 keV ^{197}Au (Coulomb excitation) and 5239.9 keV ^{15}O transitions during the measurement. The Ge crystals were gain matched by using the 279 and 547 keV transitions in ^{197}Au, the 937 keV transition of ^{18}F populated in the ^{3}He(^{16}O, p) ^{18}F reaction, and the 5.24 MeV ^{15}O line. The add-back energy spectrum was then linearly calibrated by using the 279 keV, 1081 keV, and 5.24 MeV transitions of ^{197}Au, ^{18}F, and ^{15}O, respectively. The consistency of the gain was confirmed by the alignment of the Doppler-shifted 6.79 MeV peak from all four Ge spectra after gain matching.

The DSL chamber was designed with a cold trap that surrounds the beam with a liquid-N_2-cooled shroud to avoid carbon buildup on the target. This was achieved by using a narrow differential pumping aperture followed by a cooled copper cylinder that enclosed the path of the beam to the target. During the measurement the DSL chamber had a pressure of 1.5–3.1×10^{-7} Torr. The implanted ^{3}He remains in the target foil at room temperature but can diffuse out at higher temperatures. Therefore, the target ladder was put in thermal contact with the copper cylinder by using BeCu springs to prevent losses of ^{3}He due to heating by bombardment with the beam. The target ladder was cooled to between −45 and −55 °C during the experiment while being bombarded with a beam power of 0.4 W. The BeCu springs provided a thermal gradient between the target ladder and the Cu cylinder to avoid carbon buildup on the target and were mounted onto a boron nitride plate for electrical isolation.

The target foil was produced at the Université de Montréal, Canada by implanting 30 keV ^{3}He into a 25.4 μm thick Au foil at a depth of $\sim$0.1 μm, which achieved a target density of 6.6×10^{17} ^{3}He/cm^2 as measured by elastic recoil detection (ERD). The foil was thick enough to stop both the ^{16}O beam and the ^{15}O recoils. The same implanted foils were used in recent femtosecond lifetime measurements with the DSL chamber at TRIUMF [21,22]. The number of elastically scattered ^{3}He detected in the Si detectors during the entire duration of the experiment was observed to be $\sim 2 \times 10^7$, which is negligible compared to the total number of implanted ^{3}He.

Charged particle ejectiles and elastically scattered ^{3}He ions were detected by using a Si detector telescope, composed of a thinner 100 μm (ΔE) and a thicker 500 μm (E) Si detector centered on the beam axis. Both were cylindrical totally depleted Si surface barrier detectors with an active area of 150 mm^2. This detector configuration was used for particle identification via the correlation of energy lost in the ΔE and the remaining energy deposited in the E Si detector. The maximum scattering angle of the α particles was determined by the position of the E Si detector to be 14.9°. The maximum recoil angle was limited to 7.7° because of its correlation with the α-scattering angle, which narrowed the Doppler-broadened γ-ray line shape.

A digital data-acquisition system was used with custom-built ten-channel TIG10 cards [23]. They amplified and digitized the signals that came from the HPGe detector as well as the Si detectors. Readout was triggered by the coincident detection of charged particles in both Si detectors.

III. ANALYSIS

The energy spectra of γ rays detected in coincidence with low-energy α particles are shown in Fig. 3. The 5.18, 5.24, 6.18, 6.79, 6.86, and 7.28 MeV states in ^{15}O were observed, all of which decay 100% of the time via γ emission. No state above the proton separation energy of 7.2970(5) MeV is known to decay by γ-ray emission with a probability exceeding 0.06%.

The Si detector telescope particle identification spectrum is shown in Fig. 4. The α-particle group was easy to separate from the three other observed charged particle groups. The energies of the α particles from the transfer reaction correlate with ^{15}O excitation energy. The gate in Fig. 4 was set on low-energy α particles which correspond to reactions that populate ^{15}O in an excited state. The low-energy α group also contains α particles from fusion evaporation reactions between the ^{16}O beam and ^{12}C target surface contaminants. Total α-particle energies were calculated by summing the energy deposited in the ΔE and E detectors. Figure 5 shows the total kinetic energies of α particles detected in coincidence with γ rays. The backgrounds under the ^{15}O γ-ray peaks were further reduced by placing gates on the total energies of the low-energy α particles.

Except for the 5.24 MeV state, all states that were directly populated have short lifetimes and emit Doppler-shifted γ rays. The 6.86 MeV state decays exclusively to the 5.24 MeV state by emitting a 1.62 MeV γ ray. The 5.18, 6.18, and 6.79 MeV states all decay directly to the ground state. The 7.28 MeV state with a lifetime of 0.7 ps decays to the ground state and the 5.24 MeV state by emitting a 2.03 MeV γ ray. The ground-state transition was not observed principally because its branching ratio is only 4% [7]. The 7.56 MeV state decays primarily via proton emission with a probability of 99.9958% [7]. It could decay to the 6.79 MeV state but with a probability

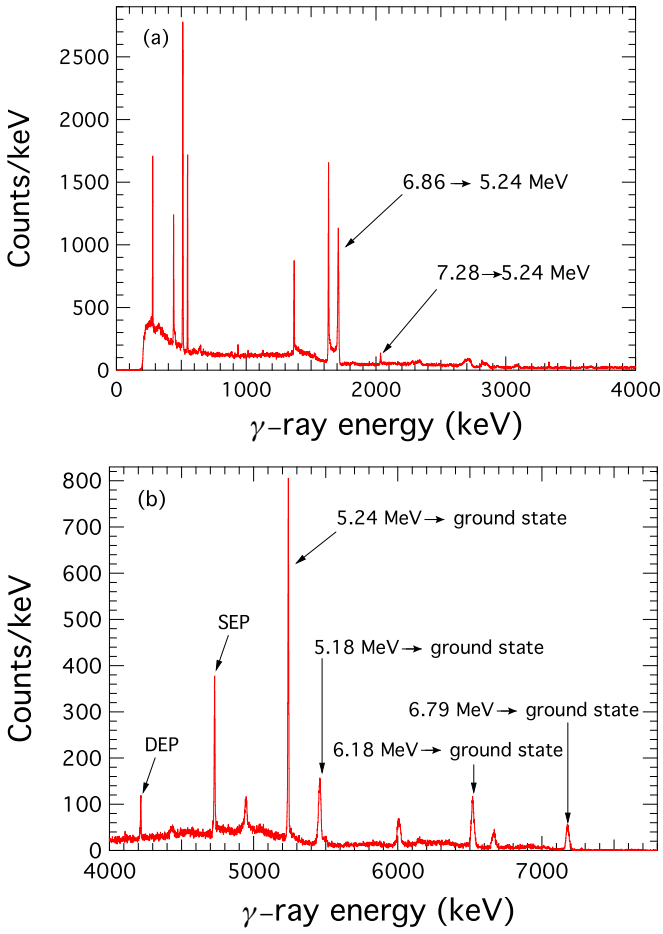

FIG. 3. (Color online) Energy spectrum of γ rays between (a) 0 and 4000 keV and (b) 4000 and 8000 keV detected in coincidence with low-energy α particles. SEP and DEP stand for the single and double escape peaks of the 5.24 MeV transition, which can also be seen for the Doppler-shifted 5.18, 6.18, and 6.79 MeV γ-ray transitions but are not labeled in every case.

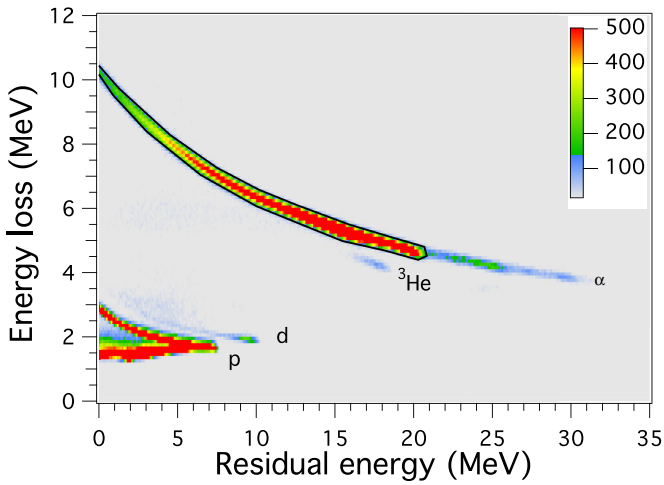

FIG. 4. (Color online) A two dimensional ΔE and E Si detector energy spectrum of charged particles detected in coincidence with γ rays. The p, d, ^{3}He, and α-particle groups are labeled. The solid curve shows the gate used to select low-energy α particles.

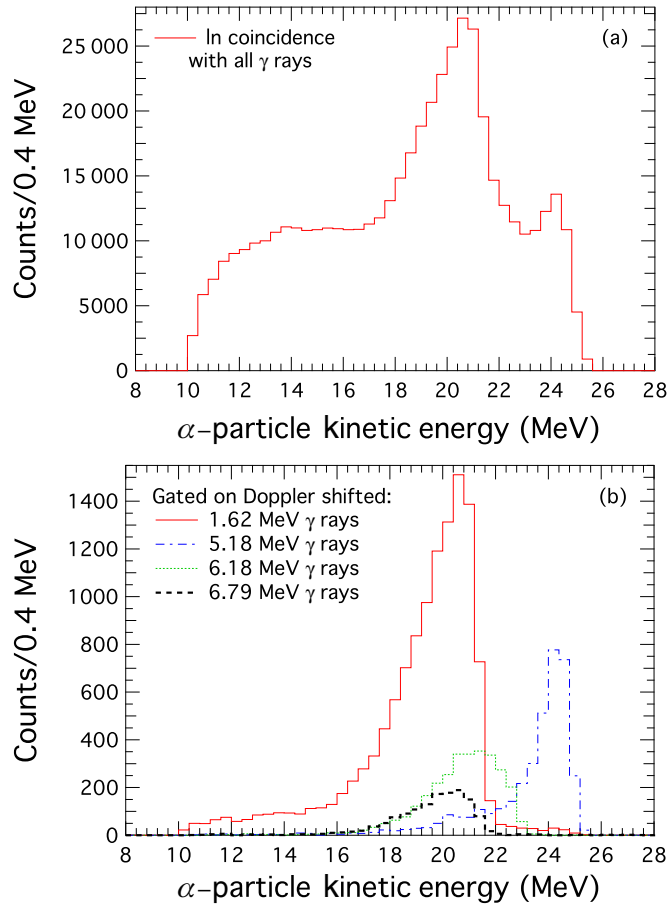

FIG. 5. (Color online) (a) Total kinetic energies deposited in the ΔE and E Si detectors by low-energy α particles that fall within the gate shown in Fig. 4. (b) Total kinetic energies of α particles inside the same gate in coincidence with the specified Doppler-shifted γ-ray transitions.

of only 0.000 98%, and since the Doppler-shifted 0.76 MeV γ ray was not observed, we are confident that there was no appreciable feeding from higher-lying states to any observed states except the 5.24 MeV level.

The 5.24 MeV state also decayed to the ground state, however given its long mean lifetime of 3 ps, an overwhelming majority of these γ rays were emitted after the ^{15}O stopped, which made feeding from a higher-lying state irrelevant. The Doppler-shifted 1.62, 6.18, and 6.79 MeV γ-ray transitions were used to determine lifetimes. It was not possible to fit the Doppler-shifted 5.18 MeV γ-ray peak since it was contaminated by the double escape peak of the Doppler-shifted 6.18 MeV γ rays as can be seen in Fig. 3(b). It proved impossible to eliminate the contribution of the double escape peak under the Doppler-shifted 5.18 MeV γ-ray peak via a gate on the total α energy since the α energies that correspond to the population of the 5.18 and 6.18 MeV states in ^{15}O, shown as the dashed-dotted and dotted histograms, respectively, in Fig. 5 overlap.

The Doppler-shifted 1.62 MeV γ-ray transition was slightly contaminated by the high-energy tail of the Doppler-shifted 1.63 MeV γ-ray transition in ^{20}Ne, a fusion evaporation

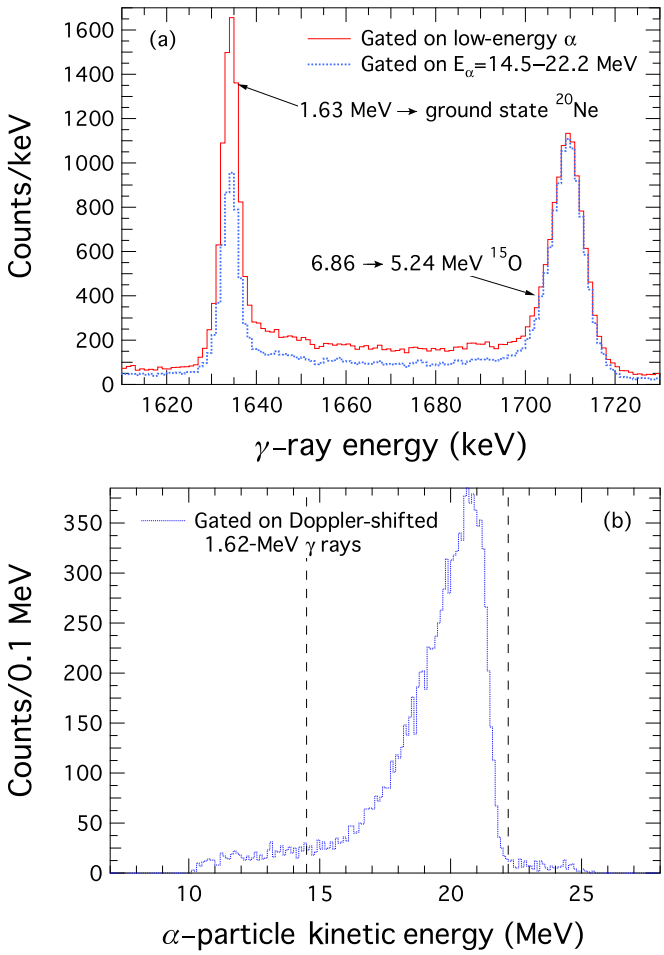

FIG. 6. (Color online) (a) Energy spectrum of γ rays detected in coincidence with all low-energy α particles (solid line) and in coincidence with α particles that have kinetic energies between 14.5 and 22.2 MeV (dotted line). (b) Kinetic-energy spectrum of α particles detected in coincidence with γ rays of energy $1696 < E_\gamma < 1723$ keV. The kinetic-energy gate applied in (a) is shown by using vertical lines.

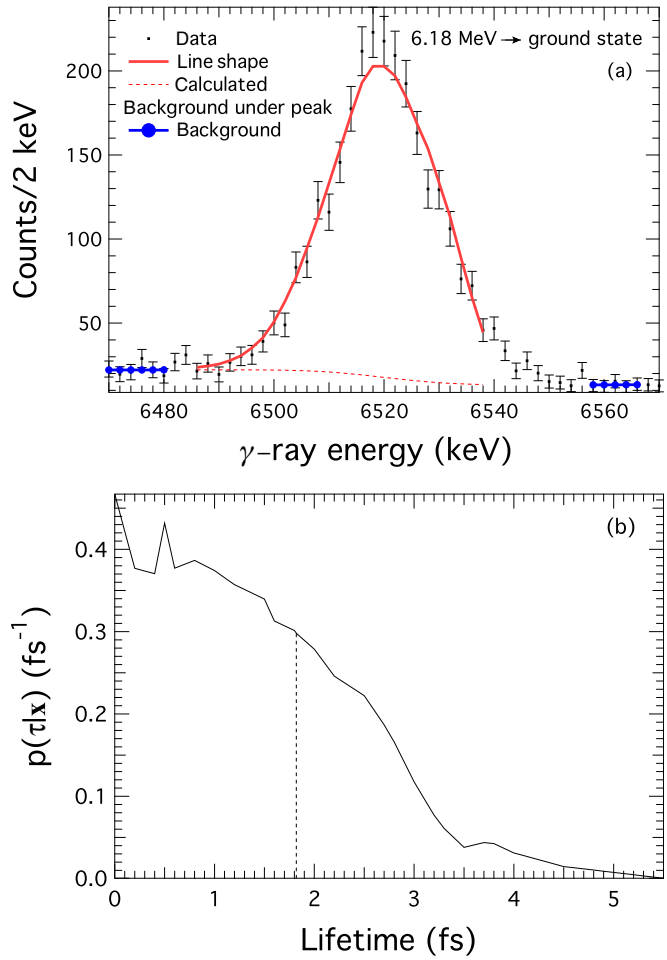

FIG. 7. (Color online) Line shape of the ground-state transition and the posterior p.d.f. $p(\tau|\boldsymbol{x})$ of the lifetime of the 6.18 MeV state. (a) Shown are the data (squares), a 0.5 fs line shape (solid line), the background fit (dotted line), and the estimated background under the peak (dashed line). (b) The posterior p.d.f. is the solid line, and the 68.3% C.L. upper limit is marked with a dashed line.

product of ^{12}C(^{16}O,2α)^{20}Ne with a lifetime of 1 ps as shown in Fig. 6(a). The α-particle energy spectrum gated on the Doppler-shifted 1.62 MeV transition and the energy gate used to reduce the ^{20}Ne γ-ray contributions are shown in Fig. 6(b). Two α particles were emitted in the fusion evaporation reactions that led to ^{20}Ne, which produced a broad α-particle kinetic-energy spectrum. In the two-body reaction that produces ^{15}O, the α particle is emitted with a unique energy for each angle, which results in a narrower kinetic-energy distribution. The low-energy threshold of the α particles associated with the Doppler-shifted 1.62 MeV γ rays was found empirically by increasing the lower limit of the energy gate and by observing when the Doppler-shifted 1.62 MeV γ-ray peak height started to decrease. The remaining ^{20}Ne γ-ray contributions under the peak were treated as part of the background. The Doppler-shifted γ rays from the 6.18 and 6.79 MeV states in ^{15}O had little background, so gating on α energy only minimally reduced the background. The background under each γ-ray peak was fit with a constant term and a complementary error function as can be seen, e.g., in Fig. 7(a).

The response function used for the Ge detector was a skewed Gaussian,

$$L(x) = (1 - h_1)G(x) + h_1 T_1(x). \tag{2}$$

$G(x)$ is a Gaussian function, $T(x)$ accounts for a low-energy tail due to incomplete charge collection and escape of secondary electrons and bremsstrahlung, and h_1 is the fractional total area under the tail. The normalized Gaussian and skewed Gaussian components were expressed as

$$G(x) = \frac{1}{\sqrt{2\pi}\sigma} \exp\left(\frac{-(x-\mu)^2}{2\sigma^2}\right), \tag{3}$$

$$T_1(x) = \frac{1}{2\beta} \exp\left(\frac{\sigma^2}{2\beta^2} + \frac{(x-\mu)}{\beta}\right) \times \operatorname{erfc}\left[\frac{1}{\sqrt{2}}\left(\frac{(x-\mu)}{\sigma} + \frac{\sigma}{\beta}\right)\right], \tag{4}$$

TABLE I. The fit results for $\sigma(E)$, $\beta(E)$, and $h_1(E)$ for E in keV.

	a	b
$\sigma(E)$ (keV)	$0.75^{+0.10}_{-0.11}$	$0.024^{+0.004}_{-0.004}$
$\beta(E)$ (keV)	$0.51^{+0.62}_{-0.61}$	$0.00078^{+0.00089}_{-0.00034}$
h_1	$0.24^{+0.06}_{-0.08}$	

where μ is the centroid of the Gaussian, σ is the standard deviation, and β tells us how much the low-energy tail differs from the low-energy side of a Gaussian, in other words it represents the "skewness" of the skewed Gaussian. A complementary error function was used for the background underneath the peak to account for the higher background on the immediately lower-energy side of the peak,

$$T_2(x) = \frac{1}{2}\mathrm{erfc}\left(\frac{(x-\mu)}{\sqrt{2}\sigma}\right). \tag{5}$$

The final fit function was

$$L(x) = (1-h_1)G(x) + h_1 T_1(x) + h_2 T_2(x), \tag{6}$$

where h_2 is the difference in background between the low- and the high-energy sides of the γ-ray peak.

The shape of the detector response function Eq. (2) was determined by the parameters σ, β, and h_1. These parameters varied with energy as

$$\sigma(E) = a + b\sqrt{E}, \tag{7}$$

$$\beta(E) = a + bE, \tag{8}$$

$$h_1(E) = a, \tag{9}$$

where a and b are intercept and slope fit parameters. The values for σ, β, and h_1 were determined by fitting the 279.01 and 547.5 keV γ rays of ^{197}Au and the 5239.9 keV ^{15}O γ ray. The constants a and b obtained are listed in Table I, and the fit of the 5239.9 keV γ-ray peak is shown in Fig. 8.

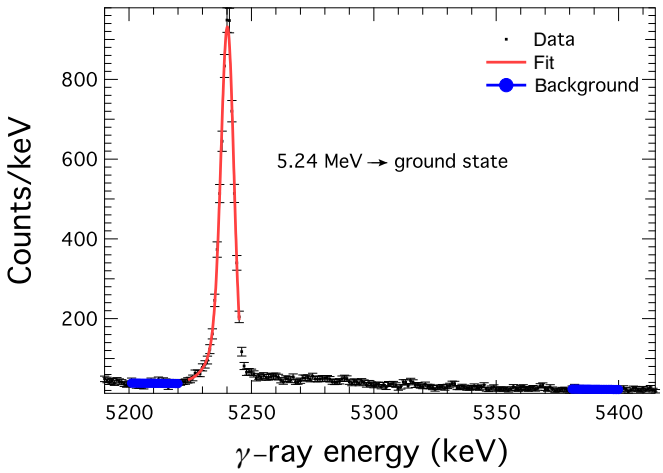

FIG. 8. (Color online) The fit to the 5.24 MeV to ground-state γ-ray transition in ^{15}O with $\tau = 3.25$ ps. The high-energy tail is due to the small number of γ rays emitted before the recoil stopped. The fit range extended only up to 5245 keV to exclude the vast majority of γ rays from unstopped recoils. The χ^2 of the fit to this peak is 13.81 for 16 degrees of freedom.

A Monte Carlo simulation was written to produce Doppler-shifted line shapes for femtosecond lifetimes. First the energy loss of the ^{16}O beam through the implanted region of the target foil before reacting as well as the beam spot size and energy spread were taken into account. Next, the ^{15}O recoil initial speed was calculated by using relativistic kinematics, which was restricted by the α-particle scattering angle. The angle of the ejectile in the c.m. $\theta_{\mathrm{c.m.}}$, which is correlated with the initial recoil angle and speed, was chosen randomly from an appropriate angular distribution given by

$$\frac{d\sigma(\theta_{\mathrm{c.m.}})}{d\Omega} = 1 + \sum_{l=1} A_l P_l(\cos\,\theta_{\mathrm{c.m.}}), \tag{10}$$

where l is the transferred orbital angular momentum, the P_l are Legendre polynomials, and A_l are their coefficients. The energy loss of the ^{15}O recoil traveling through the target foil before emitting the γ ray was calculated by using stopping powers from SRIM [24]. The Doppler-shifted energy of the γ ray was determined by the speed and the angle of ^{15}O as can be seen in Eq. (1). The angle of the γ ray was chosen from an isotropic distribution in the c.m. system since the results differed negligibly from those calculated with an anisotropic distribution. The angle-dependent Ge detector efficiencies were used to determine the acceptance or rejection of each γ-ray event. The detector response was added to the Doppler-shifted γ-ray energy at the end. The uncertainty in lifetime due to the detector response was negligible.

This code was written for the special case of high-speed recoils with femtosecond lifetimes. Therefore we expect negligible nuclear scattering of the recoil before emitting the γ ray. In this code the multiple scatterings of the ejectiles in the Au target and in the Si detectors were neglected. This meant that the program failed to account for the detection of large angle ejectiles that scattered back into the Si detectors, which were correlated with high-energy recoils. This resulted in a line shape that undershot the data on the high-energy end. Due to this we omitted fitting the high-energy tail of the line shape to the data. A background was added to the simulated line shape, and the amplitude was varied to fit the data. The best amplitude for each simulated line shape was found by using the maximum likelihood method [25]. The background was fit separately from the line shape by using the surrounding parts of the spectrum to increase the fidelity with the sum of a linear function and a complementary error function, which was used to account for the elevated lower-energy background of the peak due to multiple Compton scattering events followed by photon escape and from the escape of photoelectrons from the Ge crystal.

The lifetime of each excited state was determined from the data by fitting the three parameters τ, E_x, and A_l. Since we are primarily interested in τ, E_x and A_l represent nuisance parameters. By using Bayesian statistics we can calculate the degree of belief for parameters $\boldsymbol{\theta}$ given data $\boldsymbol{x}$ from the posterior probability density function (p.d.f.) $p(\boldsymbol{\theta}|\boldsymbol{x})$ [25]. From Bayes's theorem the posterior p.d.f. is

$$p(\boldsymbol{\theta}|\boldsymbol{x}) = \int p(\boldsymbol{\theta},\boldsymbol{\nu}|\boldsymbol{x})d\boldsymbol{\nu} \tag{11}$$

$$= \frac{\int L(\boldsymbol{x}|\boldsymbol{\theta},\boldsymbol{\nu})\pi(\boldsymbol{\theta})\pi(\boldsymbol{\nu})d\boldsymbol{\nu}}{\iint L(\boldsymbol{x}|\boldsymbol{\theta}',\boldsymbol{\nu})\pi(\boldsymbol{\nu})\pi(\boldsymbol{\theta}')d\boldsymbol{\nu}\,d\boldsymbol{\theta}'}, \tag{12}$$

where $p(\boldsymbol{\theta},\boldsymbol{\nu}|\boldsymbol{x})$ is the posterior p.d.f. with nuisance parameters $\boldsymbol{\nu}$, the likelihood $L(\boldsymbol{x}|\boldsymbol{\theta},\boldsymbol{\nu})$ is the joint p.d.f. for the experimental data $\boldsymbol{x}$ as a function of $\boldsymbol{\theta}$ and $\boldsymbol{\nu}$, and $\pi(\boldsymbol{\nu})$ and $\pi(\boldsymbol{\theta})$ are the prior p.d.f.s for $\boldsymbol{\nu}$ and $\boldsymbol{\theta}$, respectively. In our case $\boldsymbol{\theta} = \tau$ and $\boldsymbol{\nu} = (E_x, A_l)$, so the p.d.f. $p(\tau, E_x, A_l|\boldsymbol{x})$ is calculated, and the most probable lifetime was obtained by integrating over the nuisance parameters,

$$p(\tau|\boldsymbol{x}) = \int\int p(\tau, E_x, A_l|\boldsymbol{x}) dE_x dA_l. \tag{13}$$

The likelihood for binned data is given in Ref. [26] by

$$L(\boldsymbol{x}|\boldsymbol{\theta},\boldsymbol{\nu}) = \prod_{i=1}^{N} \frac{\eta_i^{n_i}}{n_i!} e^{-\eta_i}, \tag{14}$$

where the data $\boldsymbol{x}$ are sorted into bin numbers $i = 1$ to N, n_i is the number of entries in bin i, and $\eta_i = \eta_i(\boldsymbol{\theta},\boldsymbol{\nu})$ is the calculated value of bin i at certain values of $\boldsymbol{\theta}$ and $\boldsymbol{\nu}$.

The Bayesian interval for a single parameter, τ in our case, is determined by requiring

$$1 - \alpha = \int_{\tau_{\rm lo}}^{\tau_{\rm up}} p(\tau|\boldsymbol{x}) d\tau, \tag{15}$$

where $1 - \alpha$ is the desired fraction of the posterior probability. $\tau_{\rm lo}$ and $\tau_{\rm up}$ were determined at the 68.3% C.L., which corresponds to a 1σ limit for one parameter [25].

There has been no evaluation since the recent precise measurements of the energies of the excited states of ^{15}O of Refs. [9,10]. There is a discrepancy in the literature that exceeds 2σ in the excitation energy of the 6.18 MeV state, and there was only one value each for the 5.24 and 6.86 MeV states in the literature. These are listed in Table II.

TABLE II. Excited-state energies E_x of ^{15}O from the literature.

Ref. [7] E_x (keV)	Ref. [9] E_x	Ref. [10] E_x
5240.9(3)		
6176.3(17)	6171.86(15)	6172.3(2)
6793.1(17)	6791.23(19)	6791.7(2)
6859.4(9)		

The prior $\pi(E_x)$ was treated differently for each excited state. For the 6.18 MeV excited state the best fit obtained by individually varying τ, E_x, and A_l was at $E_x = 6173.5$ keV. This energy falls in between the values presented in Refs. [7,9,10] (listed in Table II) and is more than 1σ away from all values. Since there is a discrepancy between all of them we chose

$$\pi(E_x = 6.18) = \begin{cases} 1 & \text{for } 6171.86 < E_x < 6176.3 \text{ keV}, \\ 0, & \text{otherwise}. \end{cases} \tag{16}$$

For the 6.79 MeV state the best fit was found for $E_x = 6793.1$ keV, which is equal to that in Ref. [7]. Therefore we adopted a Gaussian distribution for the prior p.d.f.,

$$\pi(E_x = 6.79) = \begin{cases} \frac{1}{\sigma\sqrt{2\pi}} \exp\left(-\frac{(E_x-\mu)^2}{2\sigma^2}\right) & \text{for } E_x > 0, \\ 0, & \text{otherwise}, \end{cases} \tag{17}$$

with $\mu = 6793.1$ and $\sigma = 1.7$ keV from Ref. [7].

The excitation energies of the 6.86 MeV and the 5.24 MeV states were varied simultaneously. The energies for the best fits from individually varying τ, E_x, and A_l were found to be $E_{x_i} = 6859.45$ and $E_{x_f} = 5240.85$ keV. Since these energies were close to those given in Ref. [7] the following Gaussian prior p.d.f. was used for the 6.86 to 5.24 MeV transition,

$$\pi(E_x = 6.86) = \begin{cases} \frac{1}{\sigma\sqrt{2\pi}} \exp\left(-\frac{(\Delta E_x - \Delta\mu)^2}{2\sigma^2}\right) & \text{for} \quad E_{x_i} > 0, \quad E_{x_f} > 0, \quad \text{and} \quad \Delta E_x > 0, \\ 0, & \text{otherwise}, \end{cases} \tag{18}$$

where $\Delta E_x = E_{x_i} - E_{x_f}$ is the energy difference in the initial and final excited states, $\Delta\mu = 6859.4 - 5240.9$ keV is the difference in the centroid energies from Ref. [7], and $\sigma = 0.95$ keV is the standard deviation of the two excited-state energies given in Ref. [7] added in quadrature.

The Legendre polynomial coefficients A_l for the α-particle angular distributions were chosen so that the cross section was non-negative. For the $E_x = 6.79$ and 6.86 MeV states, $l = 2$, and for the $E_x = 6.18$ MeV state, $l = 1$. The limits of the coefficients such that $\frac{d\sigma}{d\Omega} \geqslant 0$ were

$$-1 \leqslant A_1 \leqslant 1 \tag{19}$$

and

$$-1 \leqslant A_2 \leqslant 2. \tag{20}$$

Apart from the physical requirement that $\tau > 0$, we assumed no prior knowledge of the p.d.f.s for τ and A_l and therefore adopted the uniform priors,

$$\pi(\tau) = \begin{cases} 1 & \text{for } \tau > 0, \\ 0 & \text{for } \tau \leqslant 0, \end{cases} \tag{21}$$

$$\pi(A_1) = \begin{cases} 1 & \text{for } -1 \leqslant A_1 \leqslant 1, \\ 0, & \text{otherwise}, \end{cases} \tag{22}$$

$$\pi(A_2) = \begin{cases} 1 & \text{for } -1 \leqslant A_2 \leqslant 2, \\ 0, & \text{otherwise}. \end{cases} \tag{23}$$

Recoils in excited states with femtosecond lifetimes decay when they are still in the implanted region of the target. Therefore the lifetime fits are sensitive to the density of the implanted layer, which affects the stopping powers. We

TABLE III. Experimental lifetimes in femtoseconds obtained here and from the literature.

	τ (fs)				
E_x (MeV)	This work	Ref. [13][a]	Ref. [15]	Ref. [14]	Ref. [7]
6.18	<2.5	$2.10^{+1.33}_{-1.32}$		<0.77	$\leqslant 2.5$[b]
6.79	<1.8	$1.60^{+0.75}_{-0.72}$	>0.42	<0.77	$\leqslant 28$[c]
6.86	$13.3^{+0.9}_{-1.2}$				16.01 ± 2.45[b]

[a]Only statistical uncertainties (90% C.L.) are reported. Systematic uncertainties were neglected in the final result.
[b]The lifetime is obtained from Ref. [28].
[c]The lifetime is obtained from Ref. [29].

adopted the two-layer medium approach and the density change due to the implanted ^{3}He described in Ref. [27].

The first layer consists of ^{3}He-implanted Au, and the second layer consists of pure Au. The implanted ^{3}He changed the stopping power of Au in two ways: there was an increase in stopping power due to the addition of ^{3}He atoms in the foil, but the ^{3}He also caused the foil to swell, thereby decreasing the density and stopping power. The swelling was treated following the method of Ref. [27]. The change in volume ΔV over the volume of the foil before implantation V is given by $\Delta V/V = Ac_0$, where c_0 is the ^{3}He peak atomic concentration and A is a material-dependent proportionality constant. Scaling the ^{3}He peak concentration of Ref. [27] to $c_0 = 0.674$ to account for the difference in the number of implanted ^{3}He and using the proportionality constant for ^{3}He in Au of $A = 0.75 \pm 0.25$ led to $\Delta V/V = 0.506 \pm 0.169$. The factor by which the density decreased was given by the quantity $1 + Ac_0 = 1.506 \pm 0.169$. The final density of the implanted layer is

$$\rho_{\text{layer 1}} = (\rho_{^3\text{He}} + \rho_{\text{Au}})/(1 + Ac_0), \tag{24}$$

where $\rho_{^3\text{He}}$ and ρ_{Au} are the mass densities of ^{3}He at the peak concentration and Au, respectively.

The first layer was assumed to have a uniform density over a rectangular profile of width $\sqrt{2\pi}\sigma$, where σ is the standard deviation of the ^{3}He distribution in Au determined from a Gaussian fit to the results of a SRIM simulation of the implantation. The stopping powers of O ions in ^{3}He-implanted Au were calculated with SRIM [24]. The first layer was a compound of ^{3}He and Au with a total swollen density of 13.23 g/cm^3 and a stoichiometric ratio of $\frac{n_{^3\text{He}}}{n_{\text{Au}}} = 2.07$, which can be calculated from c_0. The ^{15}O recoils decayed in the implanted region for all three states whose lifetimes were measured. There were two systematic uncertainties associated with the stopping powers: one was due to the uncertainty in target density because of the uncertainty in A, and the other was due to the uncertainty in the individual SRIM stopping powers. The uncertainty in A affected the stopping powers by $\sim \pm 10\%$. The SRIM uncertainties were determined by comparing them with experimental stopping powers obtained for O ions in Au at our energy of interest. We estimated this uncertainty to be $\pm 2.5\%$.

The uncertainty in beam energy E_b and the Si detector distance d_{Si} had similar effects on the inferred lifetime and therefore were treated together to find a joint systematic uncertainty. The Si detector distance determined the maximum α-ejectile scattering angle and hence affected the initial ^{15}O angular and speed spreads.

IV. RESULTS

The lifetime results and systematic uncertainties obtained for the 6.18, 6.79, and 6.86 MeV excited states in ^{15}O are summarized in Table III; the separate contributions to the uncertainties are specified in Table IV. We report the lifetime uncertainty due to the excitation energy and ejectile angular distribution Legendre polynomial coefficient, the uncertainty due to the beam energy and the Si detector distance, the uncertainty due to the stopping power, and that due to the swelling of the implanted layer in this order. All errors shown are at the 68.3% C.L. The total uncertainty in the lifetime was calculated by adding these uncorrelated errors in quadrature.

The calculated line shape of the 6.18 MeV to ground-state transition shown in Fig. 7(a) is for a lifetime of 0.5 fs obtained by independently varying E_x and A_l. However, the most probable value obtained globally from the posterior p.d.f. $p(\tau|\boldsymbol{x})$, over which the nuisance parameters are marginalized, is 0 fs with an upper limit of 1.86 fs at the 68.3% C.L. as shown in Fig. 7(b). There is a local maximum in the posterior p.d.f. at 0.5 fs almost as probable as 0 fs. Therefore we could only determine an upper limit on the lifetime. The result for this state, which includes all systematic uncertainties listed in Table IV is an upper limit of $\tau < 2.5$ fs (68.3% C.L.). The upper limit on this lifetime is in agreement with the results of Refs. [13,14].

Figure 9 shows the fit results for the 6.79 MeV to ground-state transition. The best fitting lifetime obtained by independently varying E_x and A_l was 0.6 fs, whose line shape is shown in Fig. 9(a). The most probable value obtained from the posterior p.d.f. $p(\tau|\boldsymbol{x})$, shown in Fig. 9(b), is 0 fs with an

TABLE IV. Contributions to the uncertainties in the lifetimes of ^{15}O excited states at the 68.3% C.L.

	Errors due to				
E_x (MeV)	E_x and A_l (fs)	E_b and d_{Si} (fs)	Stopping powers (fs)	Swelling constant (fs)	Total (fs)
6.18	$^{+1.86}_{-0.00}$	$^{+1.31}_{-0.00}$	$^{+0.58}_{-0.00}$	$^{+0.78}_{-0.00}$	$^{+2.47}_{-0.00}$
6.79	$^{+1.42}_{-0.00}$	$^{+1.08}_{-0.00}$	$^{+0.10}_{-0.00}$	$^{+0.45}_{-0.00}$	$^{+1.84}_{-0.00}$
6.86	± 0.61	$^{+0.27}_{-0.77}$	$^{+0.12}_{-0.38}$	$^{+0.53}_{-0.56}$	$^{+0.86}_{-1.19}$

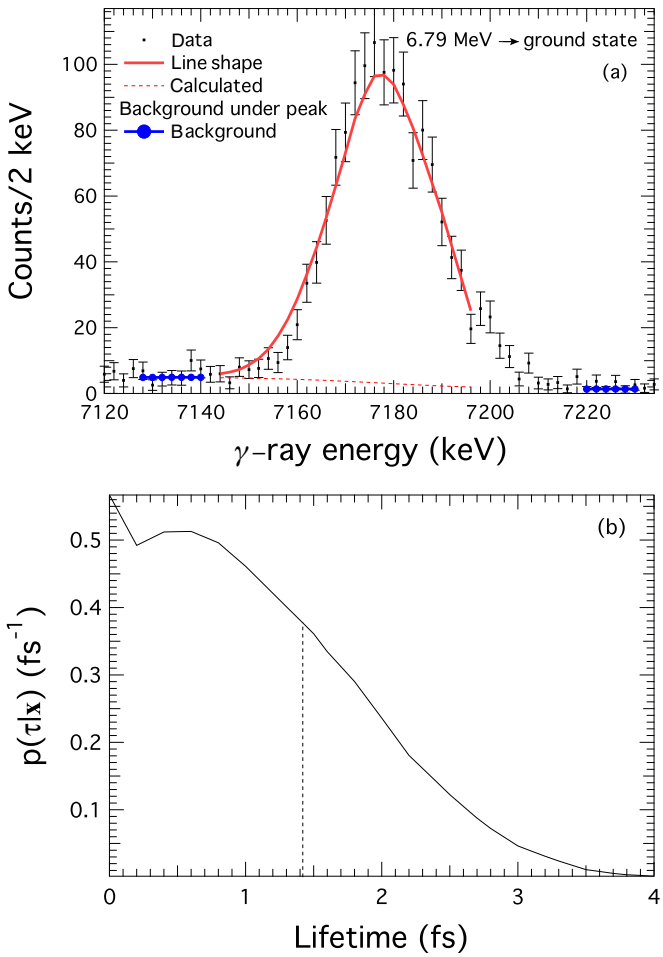

FIG. 9. (Color online) Line shape of the ground-state transition and the posterior p.d.f. $p(\tau|\boldsymbol{x})$ of the lifetime of the 6.79 MeV state. (a) Shown are the data (squares), a 0.6 fs line shape (solid line), the background fit (dotted line), and the estimated background under the peak (dashed line). (b) The posterior p.d.f. is the solid line, and the 68.3% C.L. upper limit is marked with a dashed line.

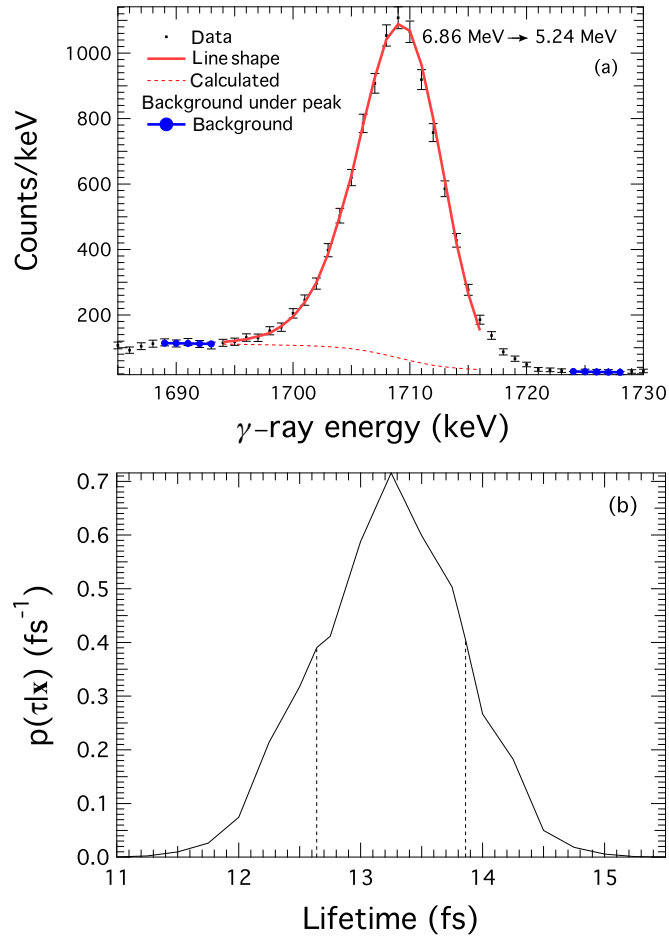

FIG. 10. (Color online) Line shape of the 6.86 to 5.24 MeV transition and the posterior p.d.f. $p(\tau|\boldsymbol{x})$ of the lifetime. (a) Shown are the data (squares), a 13.25 fs line shape (solid line), the background fit (dotted line), and the estimated background under the peak (dashed line). (b) The posterior p.d.f. is the solid line, and the 68.3% C.L. interval is marked with dashed lines.

upper limit of 1.42 fs at the 68.3% C.L. A local maximum in the posterior p.d.f. at 0.6 fs is not so prominent for this transition. The resulting lifetime of this state, which includes all systematic uncertainties listed in Table IV, is an upper limit of $\tau < 1.8$ fs (68.3% C.L.), completely consistent with Refs. [13–15].

We find a lifetime of $\tau = 13.3^{+0.9}_{-1.2}$ fs for the 6.86 MeV excited state in ^{15}O, which is in agreement with Ref. [7] but a factor of 2 more precise. The best lifetime obtained by independently varying E_x and A_l was 13.00 fs, shown in Fig. 10(a), but the most probable value obtained from the posterior p.d.f. $p(\tau|\boldsymbol{x})$ shown in Fig. 10(b) was 13.25 fs.

Our largest source of error for the 6.18 and 6.79 MeV states is due to the uncertainty in the excitation energies of ^{15}O and the angular distributions of the α ejectiles. A new evaluation of the energies of the 5.24, 6.18, 6.79, and 6.86 MeV excited states of ^{15}O would be most welcome. At the cost of introducing additional theoretical uncertainty, it is possible to restrict the A_l values of the ejectile angular distributions by using results from direct reaction model calculations.

The errors due to the target densities and stopping powers were minor sources of uncertainties for the 6.18 and 6.79 MeV states. The electronic stopping powers relevant to the swift heavy ions studied here have small uncertainties compared to the nuclear stopping powers needed in Refs. [13,14], and the error due to the uncertainty in the target density of the implanted region was small.

Both of the previous lifetime measurements neglected the systematic uncertainties in stopping powers due to the density of the target and the uncertainty due to SRIM stopping powers in the final presentation of their results. For the targets, ^{14}N-implanted Ta foils were used, but the authors assumed a target density equal to that of pure Ta. Reference [13] reports an increase in the inferred lifetime of 100% if the TaN density was used, and Ref. [14] reports a mere 2% increase for this case. In the femtosecond lifetime regime the recoils are still traveling in the implanted region of the target foil when γ-ray emission occurs and the stopping powers are very sensitive to the target

composition and density. The authors of Ref. [13] assert that the correct target density was assumed since they measured the lifetime of the 5.18 MeV state to be $9.67^{+1.34}_{-1.24}$ fs (90% C.L.), which is in agreement with 8.2 ± 1.0 fs, the value from Ref. [7]. The authors of Ref. [14], having measured a lifetime of 8.4 ± 1.0 fs for the 5.18 MeV state, used the same argument. Here we included all identified systematic uncertainties and achieved a factor of 2 more precise results for the lifetime of the 6.86 MeV state than the evaluation of Ref. [7].

V. SUMMARY AND CONCLUSION

The 6.18, 6.79, and 6.86 MeV excited states in ^{15}O were populated in the ^{3}He(^{16}O,α)^{15}O reaction at a beam energy of 50 MeV by using a ^{3}He-implanted Au target foil. The lifetimes of the states were measured from the Doppler shift of the γ rays emitted in the decay of the ^{15}O recoils. Deexcitation γ rays were detected with a HPGe clover detector. The line shape of the γ ray depended on the lifetime of the excited state; therefore we performed a line-shape analysis by using the Doppler-shift attenuation method. A Monte Carlo simulation was written to produce the line shapes for varying lifetimes. The lifetime was determined by the maximum likelihood method, and systematic errors were estimated by marginalizing over nuisance parameters.

In the present work we were not able to measure a finite lifetime for the 6.79 MeV state in ^{15}O. We were limited by statistics, but the lifetime may well be too short to be measured by any known method. The upper limit of the lifetime $\tau <$ 1.84 fs is equivalent to a lower limit on the width Γ of 0.44 eV. This is consistent with the widths obtained through R-matrix fits of the S factor of the ^{14}N(p,γ)^{15}O reaction, which were 1.75 ± 0.6 eV [8], 0.8 ± 0.4 eV [9], and 0.9 ± 0.2 eV [12]. However, the present result also does not contradict the large width $\Gamma = 6.3$ eV [6], which justified the conclusion that the capture to the ground state of ^{15}O was an equal contributor to the S factor at zero energy.

In addition to the 6.79 MeV state we report measurements of the lifetimes of the 6.18 and 6.86 MeV states in ^{15}O of $\tau < 2.5$ and $\tau = 13.3^{+0.9}_{-1.2}$ fs, respectively. Our measured lifetime of the 6.86 MeV state is in agreement with and more precise than the evaluation of Ref. [7].

We can potentially further improve the analysis by reducing the uncertainty on the ejectile angular distribution by constraining it with theoretical calculations, although this would introduce additional theoretical uncertainty. A measurement of the angular distribution would provide even better constraints. A new evaluation of ^{15}O excited-state energies would also greatly reduce the uncertainty in the lifetimes. In a future DSAM experiment one could change the setup to constrain the ^{15}O angle through a transmission measurement with a recoil separator instead of via the detection of α particles. The authors of Ref. [30] report a lifetime measurement in which the target foil was thin enough for the recoils to pass through, allowing for the separation of the beam and recoils with a mass spectrometer and gating the γ rays on the recoil of interest. This approach is very effective in suppressing background and might constrain the recoil angle enough to enable measurements of lifetimes below 1 fs.

ACKNOWLEDGMENTS

N.G. was generously supported by the DOC-FFORTE of the Austrian Academy of Sciences. We would like to thank the TIGRESS team for their help in setting up the Ge detector and DAQ system and their helpful discussions on the γ-ray data analysis. We are grateful to J. S. Forster for his assistance and thank M. Chicoine and S. Gujrathi of the Université de Montreal for carrying out the ^{3}He implantations and for measuring the depth profiles by ERD. The authors acknowledge the generous support of the Natural Sciences and Engineering Research Council of Canada. TRIUMF receives federal funding via a contribution agreement through the National Research Council of Canada.

[1] C. E. Rolfs and W. S. Rodney, *Cosmos in the Cauldron* (University of Chicago Press, Chicago, 1988).
[2] S. degl'Innocenti, G. Fiorentini, B. Ricci, and F. L. Villante, Phys. Lett. B **590**, 13 (2004).
[3] B. Chaboyer, P. Demarque, P. J. Kernan, and L. M. Krauss, Astrophys. J. **494**, 96 (1998).
[4] W. C. Haxton, R. G. Hamish Robertson, and A. M. Serenelli, Annu. Rev. Astron. Astrophys. **51**, 21 (2013).
[5] E. G. Adelberger, A. García, R. G. H. Robertson, K. A. Snover, A. B. Balantekin, K. Heeger, M. J. Ramsey-Musolf, D. Bemmerer, A. Junghans, C. A. Bertulani *et al.*, Rev. Mod. Phys. **83**, 195 (2011).
[6] U. Schröder, H. W. Becker, G. Bogaert, J. Gorres, C. Rolfs, H. P. Trautvetter, R. E. Azuma, C. Campbell, J. D. King, and J. Vise, Nucl. Phys. A **467**, 240 (1987).
[7] F. Ajzenberg-Selove, Nucl. Phys. A **523**, 1 (1991).
[8] C. Angulo and P. Descouvemont, Nucl. Phys. A **690**, 755 (2001).
[9] A. Formicola, G. Imbriani, H. Costantini, C. Angulo, D. Bemmerer, R. Bonetti, C. Broggini, P. Corvisiero, J. Cruz, P. Descouvemont *et al.*, Phys. Lett. B **591**, 61 (2004).
[10] G. Imbriani, H. Costantini, A. Formicola, A. Vomiero, C. Angulo, D. Bemmerer, R. Bonetti, C. Broggini, F. Confortola, P. Corvisiero *et al.*, Eur. Phys. J. A **25**, 455 (2005).
[11] R. C. Runkle, A. E. Champagne, C. Angulo, C. Fox, C. Iliadis, R. Longland, and J. Pollanen, Phys. Rev. Lett. **94**, 082503 (2005).
[12] M. Marta, A. Formicola, G. Gyürky, D. Bemmerer, C. Broggini, A. Caciolli, P. Corvisiero, H. Costantini, Z. Elekes, Z. Fülöp *et al.*, Phys. Rev. C **78**, 022802 (2008).
[13] P. F. Bertone, A. E. Champagne, D. C. Powell, C. Iliadis, S. E. Hale, and V. Y. Hansper, Phys. Rev. Lett. **87**, 152501 (2001).
[14] D. Schürmann, R. Kunz, I. Lingner, C. Rolfs, F. Schümann, F. Strieder, and H.-P. Trautvetter, Phys. Rev. C **77**, 055803 (2008).
[15] K. Yamada, T. Motobayashi, H. Akiyoshi, N. Aoi, Z. Fülöp, T. Gomi, Y. Higurashi, N. Imai, N. Iwasa, H. Iwasaki *et al.*, Phys. Lett. B **579**, 265 (2004).
[16] T. K. Alexander and J. S. Forster, *Advances in Nuclear Physics*, Vol. 10 (Plenum, New York, 1968), pp. 197–320.

[17] C. E. Svensson, G. Hackman, C. J. Pearson, M. A. Schumaker, H. C. Scraggs, M. B. Smith, C. Andreoiu, A. Andreyev, R. A. E. Austin, G. C. Ball *et al.*, Nucl. Instrum. Methods Phys Res., Sect. A **540**, 348 (2005).

[18] S. Agostinelli, J. Allison, K. Amako, J. Apostolakis, H. Araujo, P. Arce, M. Asai, D. Axen, S. Banerjee *et al.* (GEANT4 Collaboration), Nucl. Instrum. Methods Phys. Res., Sect. A **506**, 250 (2003).

[19] M. A. Schumaker, G. Hackman, C. J. Pearson, C. E. Svensson, C. Andreoiu, A. Andreyev, R. A. E. Austin, G. C. Ball, D. Bandyopadhyay, A. J. Boston *et al.*, Nucl. Instrum. Methods Phys. Res., Sect. A **570**, 437 (2007).

[20] M. Saha Sarkar, R. Kshetri, R. Raut, A. Mukherjee, M. Sinha, M. Ray, A. Goswami, S. Roy, P. Basu, H. Majumder *et al.*, Nuc. Instrum. Methods Phys. Res., Sect. A **556**, 266 (2006).

[21] R. Kanungo, T. K. Alexander, A. N. Andreyev, G. C. Ball, R. S. Chakrawarthy, M. Chicoine, R. Churchman, B. Davids, J. S. Forster, S. Gujrathi *et al.*, Phys. Rev. C **74**, 045803 (2006).

[22] S. Mythili, B. Davids, T. K. Alexander, G. C. Ball, M. Chicoine, R. S. Chakrawarthy, R. Churchman, J. S. Forster, S. Gujrathi, G. Hackman *et al.*, Phys. Rev. C **77**, 035803 (2008).

[23] J. P. Martin, C. Mercier, N. Starinski, C. J. Pearson, and P. A. Amaudruz, IEEE Trans. Nucl. Sci. **55**, 84 (2008).

[24] J. F. Ziegler, M. D. Ziegler, and J. P. Biersack, Nucl. Instrum. Methods Phys. Res., Sect. B **268**, 1818 (2010).

[25] C. Amsler, M. Doser, M. Antonelli, D. M. Asner, K. S. Babu, H. Baer, H. R. Band, R. M. Barnett, E. Bergren *et al.* (Particle Data Group), Phys. Lett. B **667**, 1 (2008).

[26] G. Cowan, *Statistical Data Analysis* (Oxford University Press, Oxford, 1998).

[27] T. K. Alexander, G. C. Ball, W. G. Davies, J. S. Forster, and I. V. Mitchell, J. Nucl. Mater. **96**, 51 (1981).

[28] J. Keinonen, M. Bister, and A. Anttila, Nucl. Phys. A **286**, 505 (1977).

[29] R. D. Gill, J. S. Lopes, O. Häusser, and H. J. Rose, Nucl. Phys. A **121**, 209 (1968).

[30] E. A. McCutchan, C. J. Lister, S. C. Pieper, R. B. Wiringa, D. Seweryniak, J. P. Greene, P. F. Bertone, M. P. Carpenter, C. J. Chiara, G. Gürdal *et al.*, Phys. Rev. C **86**, 014312 (2012).